Doukari Michaela, Ph.D. Candidate,
Marine Sciences Dep., University of the Aegean
m.doukari@marine.aegean.gr
Papakonstantinou Apostolos, Post-Doc. Researcher
Geography Dep., University of the Aegean
apapak@geo.aegean.gr
Topouzelis Konstantinos, Assistant Professor.
Marine Sciences Dep., University of the Aegean
topouzelis@marine.aegean.gr

Fighting the sunglint removal in UAV images

Abstract

Sun glint is the phenomenon that appears at the sea surface by the reflection of the sunlight, on remote sensing images. Sun glint removal techniques, in high spatial resolution satellite images, have been presented previously, with the use of Near Infrared (NIR) band.

In this paper, the efficiency of the sun glint removal technique in a UAV orthophoto map is examined. Initially, a script was created using the programming language R, with steps adjusted to the methodology. The script was applied to a WorldView-2 image, a CASI airborne image, and an orthophoto map created from a multispectral camera on an Unmanned Aerial Vehicle (UAV). The visible bands (RGB) and a Near-infrared band (NIR) were used as input data. Samples on regions that contain intense, moderate and less sun glint were selected on the images. The linear regression between the visible bands with the NIR band released the necessary factors for the sun glint removal equation.

The results showed that deglint methodology is efficient for the satellite and CASI image. The corrected images contain information on the benthic habitats not apparent in the original images. In the multispectral orthophoto map case a variation of the methodology was used and its efficiency is under investigation.

Keywords: *Sun glint, UAV images, Aerial images, Remote Sensing, R*

Introduction

When the light enters to a not smooth surface that its dimensions are comparable to the wavelength, it is reflected in several directions with a distribution practically independent of the angle of incidence. This diffuse reflection is produced due to the roughness of the surface, resulting in multiple reflections in various angles from the abnormalities within the material.

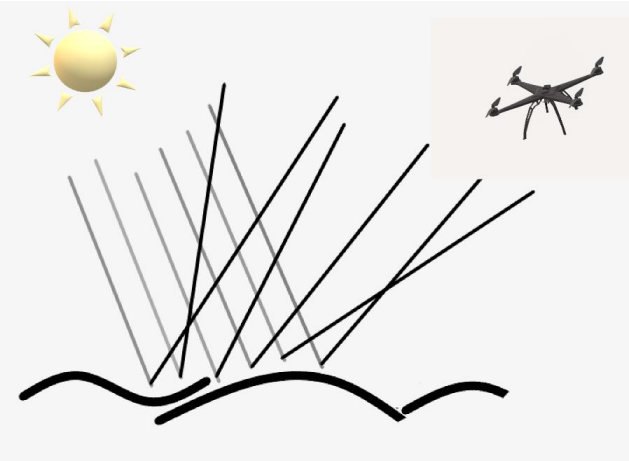

Figure 1 Sun light reflections on a wavy sea

The combination of the atmospheric and the water surface conditions with the solar and view angle during image acquisition caused the sun glint effect (Anggoro, Siregar, & Agus, 2016; Khattak, Vaughan, & Cracknell, 1991; Ottaviani et al., 2008; Mount, 2005). Sun glint is the reflection of scattered sunlight in suitably oriented tilted facets of the water surface into the sensor (Cornara, Pirondini, & Palmade, 2017). The sun glint arises from single or multiple reflections of the direct downward sunlight on the water body (Cornara et al., 2017). The intensity of sun glint depends on the ocean surface roughness and on the imaging geometry (Sun position, sensor viewing direction and field of view) (Cornara et al., 2017; Harmel, Chami, Tormos, Reynaud, & Danis, 2018). Thus, imaging data acquired over water are corrupted by sun glint contamination. In our case, as a sun glint, we study solely the phenomenon based on the water body direct beam reflection.

In satellite installations sunlight is a critical parameter for a) satellite orbits b) satellite global coverage, c) satellite altitude range d) satellite sun-synchronous orbit e) instruments (sensors) design and specifications and c) instruments installation onto the satellite. The criticality of the above-mentioned parameters derives from the sun glint impact on visible channels of the solar ray reflection on the water surface. This constraint in the Sentinel-3 installation was overcome thanks to the concurrent optimization of the orbit parameters, the Local Time at Descending Node (LTDN), and the OLCI instrument FoV definition (Cornara et al., 2017).

There are several available sun glint removal methods for open ocean imaging and higher resolution coastal and aerial applications (Kay, Hedley, & Lavender, 2009; Overstreet & Legleiter, 2017). In open ocean images, statistical models that combine the sun glint distribution with the slopes on the sea surface (Cox & Munk, 1954) and radiative transfer models (Ottaviani et al., 2008), are used for the prediction of the reflected sun light. While, in high-resolution imagery more methods use the three optical spectrum bands and a near-infrared (NIR) band (Hedley, Harborne, & Mumby, 2005; Hochberg, Andréfouët, & Tyler, 2003) to remove sun glint effect. These methodologies use the assumption that the values of the NIR band are zero for the entire image. The results of these methodologies have shown an improvement in marine habitat classification and better image interpretation, as the marine features are better delineated, and their contrast is increased. However, a method that uses the oxygen absorption feature at 760 nm, instead of NIR band is also available (Overstreet & Legleiter, 2017). In UAV multispectral images, automated algorithms that detect and remove sun glinted images are available (Ortega-Terol, Hernandez-Lopez, Ballesteros, & Gonzalez-Aguilera, 2017).

In the present paper, Hedley's sun glint removal method is developed with the use of programming language R, to produce an automated process and investigate its effectiveness, in different data types and mainly in a multi-spectral UAV orthophoto map.

Methodology:

The workflow process that follows is based on the steps of Hedley's methodology for the removal of sun glint from high-resolution images. This methodology established the linear relationships between NIR and visible bands using linear regression based on a sample of the image pixels (Hedley et al., 2005). It doesn't require the masking of land or clouds because the samples are selected by the user and areas like that are avoided. Also, the methodology can be performed using image digital numbers, thus the conversion of the pixel values into radiance is not necessary. The samples of the affected sun glint regions are suggested to be large enough to reduce the effect of random variations. The selection of different regions on the image, with a range of sun glint, will fill the lower, medium and the upper end of the regression and the slope will be established. The application of the following equation (1), creates deglinted bands of a multispectral image. The equation must be applied to any band we want to deglint.

$$R'_i = R_i - b_i (R_{NIR} - Min_{NIR}) \qquad (1)$$

In this equation, the pixel values of the selected sun glint samples Ri of an i band are corrected by the production of the regression slope bi. The slope has been calculated by the linear regression between pixel values of visible and NIR bands, of the samples. The difference between the pixel values of NIR band with the min value of the NIR band in a deep-water area is also required. Ri' is the corrected pixel values of i band. Hedley's methodology has been successfully tested in high-resolution satellite and airborne imagery.

The need to repeat the methodology in many coastal mapping applications, has led to the creation of an automated process with the use of the programming language R. R is a free programming language with many capabilities and widely used from researchers in a range of tasks, in recent years. R provides a plethora of packages for raster and vector manipulation and visualization. The steps of the sun glint removal methodology were applied to a script, creating an automated sun glint removal tool that can be used in high-resolution aerial imagery. This process was applied in three different case studies of high-resolution images, a satellite, an airborne and a UAV image, to test the effectiveness of the method in different resolutions.

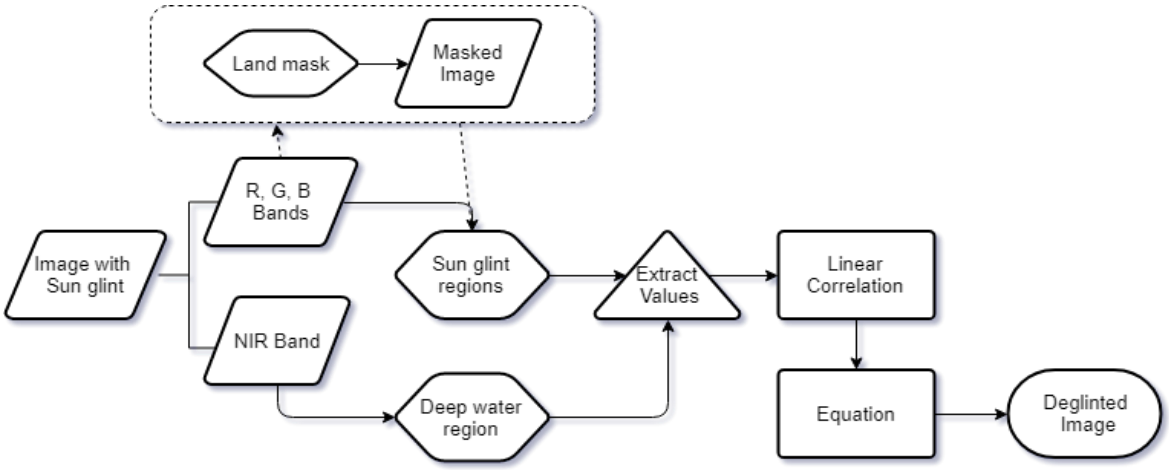

Figure 2 Methodology Workflow

Sun glint removal is a pre-processing step of multispectral images which is necessary when the amount of sun glint prevents the visibility of the sea bottom, usually in cases of marine habitat mapping. The methodology uses the Red, Green, Blue visible bands and a Near-Infrared (NIR) band of a multispectral image, so these bands were selected from each image and inserted into the script, as a raster brick with a .tiff format. All bands must have the same size of a pixel, number of colors, extension, and reference to be comparable to each other. The bands were masked with a land mask which consists of 0 and 1 values for the land and the sea, respectively. A mask can be created with the use of a threshold of the NIR band for the separation of the land from the sea or with the use of a polygon which describes the land and excludes it from the image. The land mask was applied to every band and a masked image was created. This step is optional, but it seems to provide a better interpretation of the result. After that, samples with a gradation of sun glint were selected on each band of the masked image. The samples must be selected carefully, not to include any on-sea surface object but different amounts of sun glint, from low to high sun glint regions. It is also important the selected regions be above a common habitat to represent areas that would not be differentiated if there was no sun glint. Three polygons which describe these regions were created and inserted into the script. The values that are included in these regions are extracted and used for the linear regressions of every visible band with the NIR band. The extracted NIR values represent the x-axis and the visible band values the y-axis. Three different slopes are calculated from this process which are main factors of the equation (1). A region of deep water is also selected from the NIR band and the extracted values are used for the calculation of the minNIR factor. The equation is applied three times to each visible band's values and three new bands are created. A true color composite of the original and the deglinted image offers a visual interpretation of the result. Additional, a transect was created along a region with increasing sun glint for the confirmation of the result. The pixel values as they move to the sun glinted areas, they tend to be bigger. A graph that visualizes the pixel values of the transect in the original image and the corrected one, was created. This graph gives a better picture of the effectiveness of the method.

Results

The creation of the sun glint removal script follows the selection of different data cases for testing its effectiveness. The first data set is an image acquired by the airborne sensor CASI,

the second is a World-View 2 image and the third a multispectral image acquired by a UAV. These datasets were selected due to the different methods they were acquired, their different resolution and amount of sun glint.

Case study 1: WorldView-2 image

The first case study is a WorldView-2 image of a coastal area from Lindos to Rhodes Island, Greece. The WorldView-2 Satellite Sensor provides a high-resolution panchromatic band of 0.46 m resolution and eight (8) multispectral bands with 1.84 m resolution. The presence of sun glint at the sea part of the image is obvious. Although the sea state is calm, a layer of sun glint doesn't allow the visibility of the benthic features. The bands 2, 3, 5 and 7 which correspond to the blue, green, red and NIR were selected for the methodology. The selection of regions without sun glint was difficult due to the biggest part of the sea except for some strips, is covered with sun glint. Also, it is not easy to distinguish the marine habitats to select regions with common features. For this reason, small polygons were selected to represent a gradation of sun glint. However, it was achieved to gather points on the lower end of the linear regressions, corresponding to areas without sun glint to define correctly the slope of the line. The correlation of visible band values with NIR band values was also high in this case. The calculated correlation between, blue and NIR band was 0.898879 and the slope (b1) 0.6296566, green and NIR band 0.890884 and the slope (b2) 1.020743, red and NIR band 0.9466773 and the slope (b3) 0.8595802.

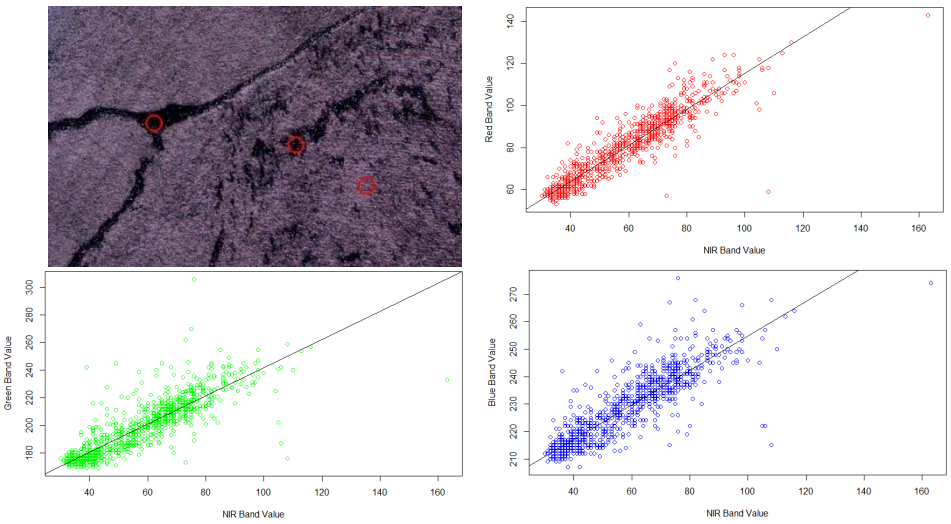

Figure 3 Selected sun glint polygons and linear regressions of RGB and NIR band values

The corrected image allows the detection of different marine habitats. Particularly, in the southern part of the image, different species of habitats are distinguished as in the coastal

northern part. The sun glint removal method has greatly improved the visibility of the seabed in that area.

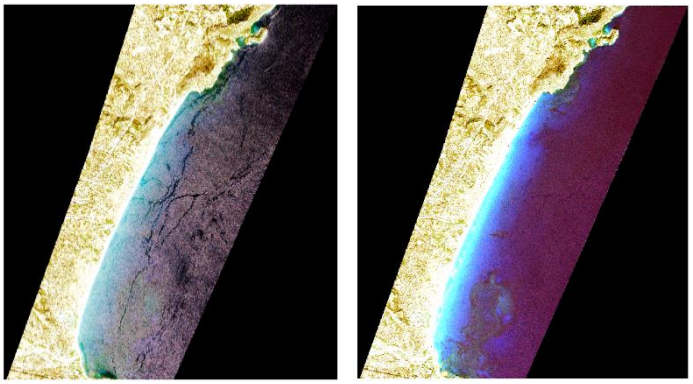

Figure 4 WorldView-2 Image with sun glint (left), Corrected WorldView-2 Image (right)

The designed transect covers a part especially with sun glint since there are no large areas in the picture without sun glint. This is likely the reason why there are no large variations in the transect values. The graphs of the three bands vary as to the range of the values but it seems that a specific pattern is followed. The red band graph presents the smallest range of values as well as larger value fluctuations.

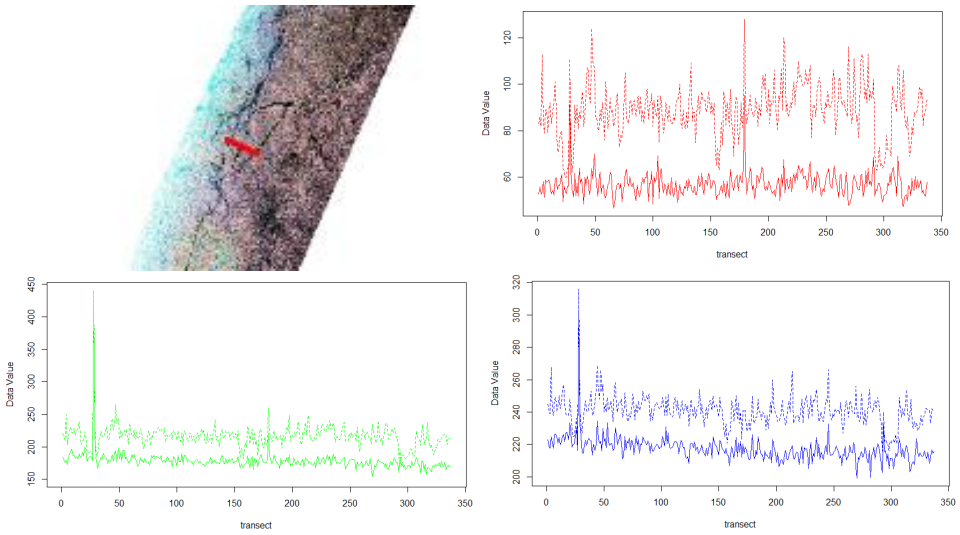

Figure 5 Transect graphs. Dotted line: The pixel values with sun glint, Continuous Line: Corrected pixel values

Case study 2: CASI (Compact Airborne Spectrographic Imager) airborne image

The second case study is an image of reefs from St John in the US Virgin Islands, acquired from CASI. The data were acquired from the airborne sensor on a light aircraft with a flight height of 1250m and a spatial resolution of 2 x 2 m (4 m2) in 19 wavebands (Indows & Edwards, 1999). The image was selected because of the amount of sun glint which prevents the visibility of reefs at the area. The sun glint is visible throughout the image with a higher concentration at the southern part, which is aggravated by the existence of waves on the sea surface. The methodology of sun glint removal requires the use of 3 visible bands and one NIR, so only four of the 19 available wavebands were used. Three different polygons on sun glint regions were

selected and their values were used for the creation of linear regressions. The correlation of the visible bands with NIR band on the selected regions was very high. The correlation between the blue band values and NIR was calculated 0.9011435 and the slope (b1) of the linear regression is 0.9857186, the green band and NIR band values were 0.9570374 and the slope (b2) 1.314436, the red band and NIR values 0.9629815 and the slope (b3) 1.207291.
The corrected image shows that the visibility of the sea bottom is increased, and the marine habitats are clearly separated. The reefs that were hidden under the sun glinted regions are now apparent. The result shows that the methodology of sun glint removal is very efficient.

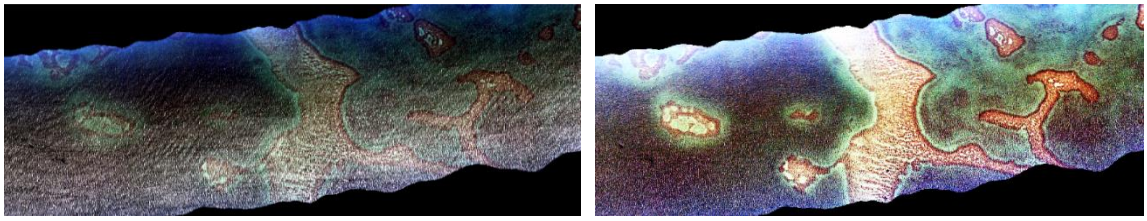

Figure 6 A true color composite of CASI airborne image with sun glint (up), Corrected CASI Image (down)

The created transect was used to compare the pixel values before and after the sun glint removal. The values in every band were used for the creation of comparing graphs. The values of the bands in the original image increase as they move towards the sun glint, as expected, while the corrected pixel values vary within a certain range of values. As shown in the charts, the values in all three bands follow a similar pattern, before and after the correction.

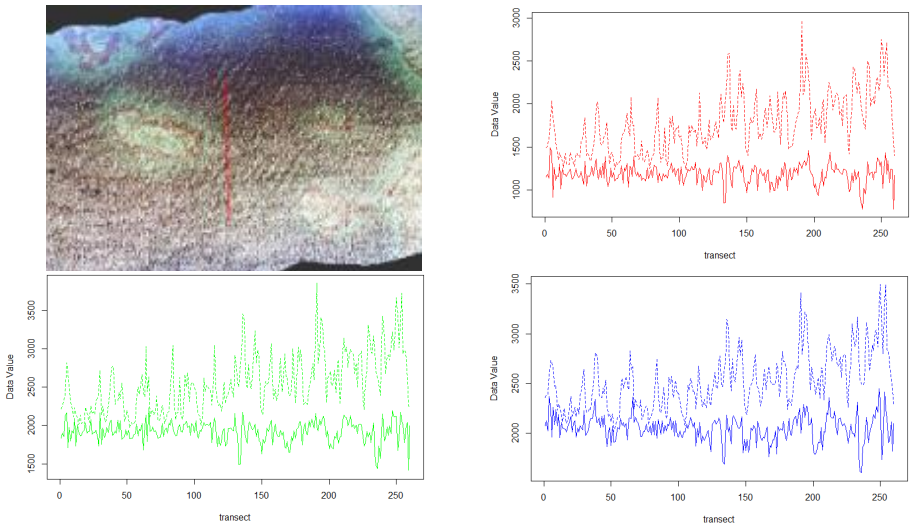

Figure 7 Transect and graphs. Dotted line: The pixel values with sun glint, Continuous Line: Corrected pixel values

Case study 3: Multispectral UAV image

The third case is a multispectral orthophoto map developed from UAV aerial images of the Salamina area, in Greece. The height flight was 100m and the used multispectral sensor is the Parrot Sequoia. This sensor features an integrated GPS/light sensor, four narrowband imagers (Green, red, red edge, near IR), and an RGB camera for digital scouting. In this case, the 3 visible bands (Red, Green, and Blue) are not available and the method was held with the use

of Green, Red, and Red Edge bands. The RGB image wasn't selected due to the small correlation between the visible bands and the NIR band. The non-calibrated RGB camera is probably the cause of it. Another limitation on the orthophoto map is that it is likely that the large concentration of sun glint at the end of the image is due to a stitching error when it was created. The correlation between the Green band and NIR is 0.7683733, the Red and NIR band is 0.8330186 and the Red Edge and NIR band is 0.7492878. The slopes of the linear regressions of each band are calculated, 1.125847, 0.5201611 and 0.9187586, respectively.

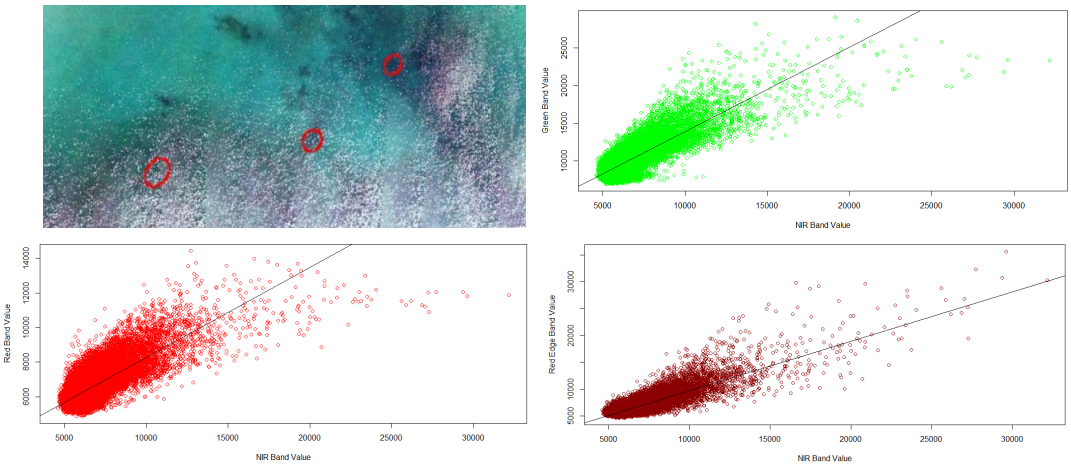

Figure 8 Selected sun glint polygons and linear regressions of Green, Red, Red Edge and NIR band values

The corrected image presents some improvements regarding the removal of some sun glint regions and the separation of marine habitats. Regions with intense sun glin, as at the edge of the orthophoto map were not completely corrected.

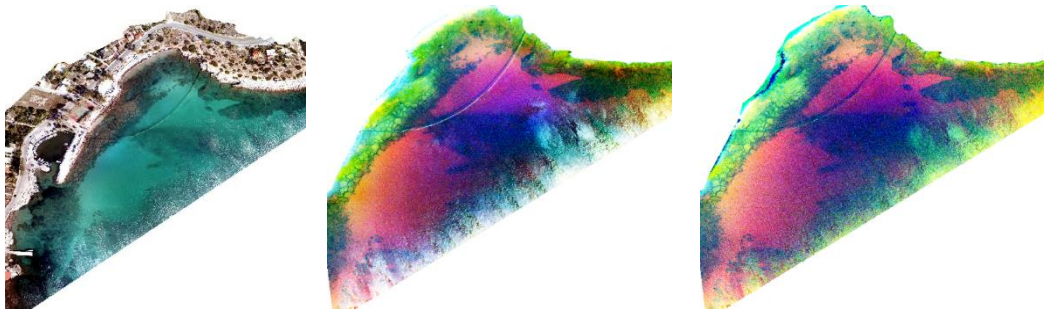

Figure 9 RGB Image (left). Green, Red, Red Edge Composite with sun glint (middle). Corrected Image (right)

Discussion and Conclusions:

In this paper we have presented an automated approach of sun glint removal techniques used in UAV data and two high resolution images of World-View 2 and CASI sensors. A land mask was applied to improve the visual interpretation of the corrected images.

Sun glint appears in all types of remote sensing data, from satellite to UAV multispectral imagery. The possibility of using different types of sensors on UAVs, such as multi-spectral sensors in combination with the high resolution acquired images, makes their use increasingly attractive, in marine applications.

Ways to avoid sun glint refer to the sun position relative to the sensor's position when considering the sea state and the wind. These parameters limit significantly, the time range of aerial data acquisition without sun glint.

The sun glint removal technique by Hochberg et al. (2003) reveal an improvement in the accuracy of benthic habitat classification, using an Ikonos image. The revised version of this method by Hedley et al. (2005), presents an improvement of the method, excluding outlier values by using linear regressions between NIR and visible bands, based on a sample of the image pixels.

The methodology of sun glint removal techniques (Hedley et al., 2005; Hochberg et al., 2003) have been shown to be effective in many types of aerial images, whereas their use is only possible in case of multispectral data, where a NIR band is available. Although, the photogrammetric algorithms that develop a UAV orthophoto map, choose the best quality images without sun glint to stitch together, if they exist.

The sun glint removal method is very effective in WorldView-2 and CASI images. The results showed that the benthic visibility and the marine habitat detection is increased in the corrected images. In the WorldView-2 image, the visibility of the marine features was increased significantly after the sun glint removal. In the CASI image, the position and the features of the reefs are clearly identified. The case of UAV orthophoto map is more complicated due to data different in the spectral bands. However, the corrected image presents several improvements compared to the original UAV orthophoto map. The sun glint removal method in UAV data can be further investigated with the use of different multispectral sensors. The automated process developed in R language, enables repeatability and quickly results export.

ACKNOWLEDGMENT

This work has been partially carried out within the framework of the Greek State Scholarship Foundation (I.K.Y.) Scholarship Programs funded by the "Strengthening Post-Doctoral Research" Act from the resources of the OP "Human Resources Development and Lifelong Learning "priority axis 6, 8, 9 and co-financed by the European Social Fund–ESF and the Greek government.

References:

Anggoro, A., Siregar, V. P., & Agus, S. B. (2016). The Effect of Sunglint on Benthic Habitats Mapping in Pari Island Using Worldview-2 Imagery. *Procedia Environmental Sciences*, *33*, 487–495. https://doi.org/10.1016/j.proenv.2016.03.101

Cornara, S., Pirondini, F., & Palmade, J. L. (2017). Sentinel-3 coverage-driven mission design: Coupling of orbit selection and instrument design. *Acta Astronautica*, *140*(August), 439–451. https://doi.org/10.1016/j.actaastro.2017.08.017

Cox, C., & Munk, W. (1954). Measurement of the Roughness of the Sea Surface from Photographs of the Sun's Glitter. *Journal of the Optical Society of America*, *44*(11), 838. https://doi.org/10.1364/JOSA.44.000838

Harmel, T., Chami, M., Tormos, T., Reynaud, N., & Danis, P. A. (2018). Sunglint correction of the Multi-Spectral Instrument (MSI)-SENTINEL-2 imagery over inland and sea waters from SWIR bands. *Remote Sensing of Environment*, *204*(March 2017), 308–321. https://doi.org/10.1016/j.rse.2017.10.022

Hedley, J. D., Harborne, A. R., & Mumby, P. J. (2005). Simple and robust removal of sun glint for mapping shallow-water benthos. *International Journal of Remote Sensing*, *26*(10), 2107–2112. https://doi.org/10.1080/01431160500034086

Hochberg, E. J., Andréfouët, S., & Tyler, M. R. (2003). Sea surface correction of high spatial resolution ikonos

images to improve bottom mapping in near-shore environments. *IEEE Transactions on Geoscience and Remote Sensing*, *41*(7 PART II), 1724–1729. https://doi.org/10.1109/TGRS.2003.815408

Indows, W., & Edwards, B. Y. a J. (1999). *Applications of Satellite and Airborne Image Data To Coastal Management Computer - Based Learning Module*.

Kay, S., Hedley, J. D., & Lavender, S. (2009). Sun glint correction of high and low spatial resolution images of aquatic scenes: A review of methods for visible and near-infrared wavelengths. *Remote Sensing*, *1*(4), 697–730. https://doi.org/10.3390/rs1040697

Khattak, S., Vaughan, R. A., & Cracknell, A. P. (1991). Sunglint and its observation in AVHRR data. *Remote Sensing of Environment*, *37*(2), 101–116. https://doi.org/10.1016/0034-4257(91)90022-X

Ortega-Terol, D., Hernandez-Lopez, D., Ballesteros, R., & Gonzalez-Aguilera, D. (2017). Automatic hotspot and sun glint detection in UAV multispectral images. *Sensors (Switzerland)*, *17*(10), 1–16. https://doi.org/10.3390/s17102352

Ottaviani, M., Spurr, R., Stamnes, K., Li, W., Su, W., & Wiscombe, W. (2008). Improving the description of sunglint for accurate prediction of remotely sensed radiances. *Journal of Quantitative Spectroscopy and Radiative Transfer*, *109*(14), 2364–2375. https://doi.org/10.1016/j.jqsrt.2008.05.012

Overstreet, B. T., & Legleiter, C. J. (2017). Removing sun glint from optical remote sensing images of shallow rivers. In *Earth Surface Processes and Landforms* (Vol. 42, pp. 318–333). https://doi.org/10.1002/esp.4063